Chem. Senses 24: 497–508, 1999

A Kinetic Model of the Transient Phase in the Response of Olfactory Receptor Neurons

Wayne M. Getz

Division of Insect Biology, ESPM, 201 Wellman Hall, University of California at Berkeley, CA 94720-3112, USA

Correspondence to be sent to: Wayne M. Getz, Division of Insect Biology, ESPM, 201 Wellman Hall, University of California at Berkeley, CA 94720-3112, USA. e-mail: getz@nature.berkeley.edu

Abstract

A model is presented that predicts the instantaneous spike rate of an olfactory receptor neuron (ORN) in response to the quality and concentration of an odor stimulus. The model accounts for the chemical kinetics of ligand–receptor binding and activation processes, and implicitly the initiation of second messenger cascades that lead to depolarization and/or hyperpolarization of the ORN membrane. Both of these polarizing processes are included in the most general form of the model, as well as a process that restores the voltage to its negative resting state. The spike rate is assumed to be linearly proportional to the level of voltage depolarization above a critical negative voltage level. The model includes the simplifying assumption that activation of bound ligand–receptor complexes by G-proteins and other enabling molecules follows a Monod function that has the ratio of enabling molecules to bound unactivated ligand–receptor complexes as its argument. Parameters are selected that provide an excellent fit of the model to previously published empirical data on the response of cockroach ORNs to pulsed 1-hexanol stimuli. The sensitivity of model output to various model parameters is investigated and changes to parameters are discussed that would improve the ability of ORNs to follow rapidly pulsed stimuli.

Introduction

Olfactory receptor neurons (ORNs) transmit information to the brain of organisms on the presence and concentration of volatile chemicals in the environment. The ORNs are the gatekeepers of olfactory perception, both in the context of which chemicals are detectable and what resolution is possible with respect to temporal variability of odors in turbulent plumes or the concentration gradients of odor fields. The neural firing or spike rate response of an ORN to a temporally and spatially varying odor stimulus results from a concatenation of biochemical, molecular conformational and flux transport processes (Hildebrand and Shepherd, 1997), each of which has various transient and steady states associated with its dynamics. Thus changes in the membrane voltage potential of an ORN in response to stimulation by an odor is a highly complex dynamical process and requires a dynamical systems model to understand fully its temporal properties. Such models usually involve differential equation descriptions of chemical or enzyme kinetic processes and current flows or voltage rates of change. Dynamical systems models can be used to obtain insights into ORN response characteristics, to generate hypotheses regarding the nature of the underlying process, or to synthesize input into neural network models of the vertebrate olfactory bulb or the crustacean antennal lobe. This synthesis function is the primary motivation for the study reported here.

Olfactory perception in an organism begins with odorant molecules or odor ligands (Hildebrand and Shepherd, 1997) penetrating the mucous layer of the olfactory epithelium in vertebrates or entering through the pores of olfactory sensilla in insects, diffusing or being transported across a liquid medium with the help of odorant binding proteins or OBPs; some of these OBPs may also be implicated in deactiving odorant molecules (Breer, 1994; Kaissling, 1998b), and then binding with receptor molecules on the dendritic membranes of ORNs. The individual receptor molecules, of which there are known to be hundreds or even thousands of types (Buck and Axel, 1991; Lancet *et al*., 1993; Reed, 1994) belong to the seven transmembrane domain, G-protein coupled family of receptor proteins. Some of these receptor molecules are known to be highly specific for particular odorants, typically those implicated in transducing sex pheromone signals in insects (Kaissling, 1987). Other receptor molecules, however, may well be generalists, able to bind to several different members of a group of ligands of the same or similar moieties (Singer and Shepherd, 1994). In this case, we expect ligand–receptor affinities or binding constants to vary among similar ligands (Lancet *et al*., 1993).

Once a ligand binds to a receptor protein, the resulting

ligand–receptor complex couples with and activates G-proteins (Firestein and Zufall, 1994). This coupling in turn initiates a second messenger cascade that ultimately causes ion channels to open and the membrane to depolarize or, in some cases, hyperpolarize, depending on which channels have been opened (Ache, 1994; Trotier, 1994). Changes in membrane polarization cause the ORNs to increase or decrease their rate of firing with respect to a cell specific background rate, depending on the concentration of the odor stimulus (Fujimura *et al*., 1991; Akers and Getz, 1992, 1993; Getz and Akers, 1993, 1997a).

For all animals, stimulation or inhibition of the ORNs is the first, or sensory transduction, phase of a multiphase perceptual process that has striking commonalities in all animals, with, of course, some notable differences among taxons with vastly different brain morphologies. The archetypal organisms for the model presented here are insects with highly developed olfactory systems, such as cockroaches and honeybees. In insects, olfactory stimuli are typically filamentous plumes of odorant molecules that have a complex spatial and temporal structure (Moore and Atema, 1991; Murlis *et al*., 1992; Dittmer *et al*., 1995; Vickers and Baker, 1994). As the odorant molecules waft around the antennae of an individual organism, the concentration of ligands available to the ORNs situated in olfactory sensilla of various types will be highly stochastic and variable over time and at different locations on the same antenna at the same point in time. The various processes altering the firing rates of the ORNs, as we show here, smooth out some of the temporal jitter in the concentration, while variations in the concentration experienced among ORNs are smoothed out by a large ensemble of ORNs converging at the next level onto orders of magnitude fewer olfactory glomeruli (Shepherd, 1972; Rospars, 1988; Boeckh *et al.*, 1990; Masson and Mustaparta, 1990; Smith and Getz, 1994; Hildebrand and Shepherd, 1997).

Mathematical models of ORNs (or, for that matter, taste receptor neurons) can focus either on the kinetics of ligand–receptor binding (Ennis, 1989, 1991; Malaka *et al*., 1995; Kaissling, 1998a, 1998b; Lánsky and Rospars, 1999) or on the alteration of receptor membrane potential and concomitant generation of action potentials (Lánsky and Rospars, 1993; Tuckwell *et al*., 1996; Vermeulen *et al*., 1996; Vermeulen and Rospars, 1998). In the former case, the assumption can be made that spike rate is an appropriate function of the number of bound ligand–receptors pairs (Getz and Akers, 1995) or models combining both aspects can be considered (Lánsky *et al*., 1994; Rospars *et al*., 1996). Here, following the ideas of Lánsky and Rospars (Lánsky and Rospars, 1999), I develop a model that combines both ligand–receptor kinetics and membrane potential dynamics. A central difficulty in this approach is to find a reasonable way to model the second messenger cascade linking the ligand–receptor dynamics to changes in membrane potential, especially when some components of this cascade are not yet well understood. I circumvent this difficulty by taking an approach inspired by consumer-resource concepts found in population ecology (Getz, 1993).

In this study, parameters in the model are selected to simulate observed data from cockroach ORNs (Lemon and Getz, 1997). Because the primary motivation for developing the model is to use it to generate realistic spike rate input for a neural network model of olfactory coding in the insect antennal lobes (Getz and Lutz, 1999), I focus on fitting the model to existing empirical data rather than capturing the details of all the processes involved with generating the response. In some cases these details are not known, particularly with regard to second messenger cascades. In other cases, the details are not necessary to capture the essential dynamic response of ORNs, and the simplest reasonable description is used; for example, I use one equation to model changes in the membrane voltage potential rather than the usual four to capture the actual spike profiles (Mascagni and Sherman, 1998). Also, if ligand–OBP dynamics occur on a much faster time scale than spike generation, then replacement of a dynamical description of ligand–OBP interaction with an appropriate static (equilibrium) value that, perhaps, includes a small time delay may be a reasonable simplification to make. Thus, although the model does provide complete insight into the processes that determine the response profiles of ORNs, the critical test of the model is how well it can generate realistic response profiles to be used as input into a network model of olfactory coding in the insect antennal lobes. As presented below, the model developed here does provide a good fit to the response of cockroach ORNs (Lemon and Getz, 1997).

Materials and methods

Modeling ligand–receptor binding kinetics

Chemical kinetic models of the rate at which populations of receptor molecules at density R on the membranes of ORNs bind to ligand messenger molecules typically begin with the assumption that monovalent ligands at density L in the perireceptor space (i.e. the space around the receptor neuron membrane where they are sufficiently proximate to interact with membrane receptor molecules) are competing for unbound receptors at density U. This implies that the density B of bound receptors is $B = R–U$, and that the reaction is of the form

$$L + U \underset{k_{-1}}{\overset{k_1}{\rightleftharpoons}} B$$

where k_1 and k_{-1} are respectively the association and disassociation rates of this reaction (Figure 1). Bound receptors, however, do not initiate second messenger cascades until they have activated a coupled G-protein (Firestein and Shepherd, 1991). The rate at which bound

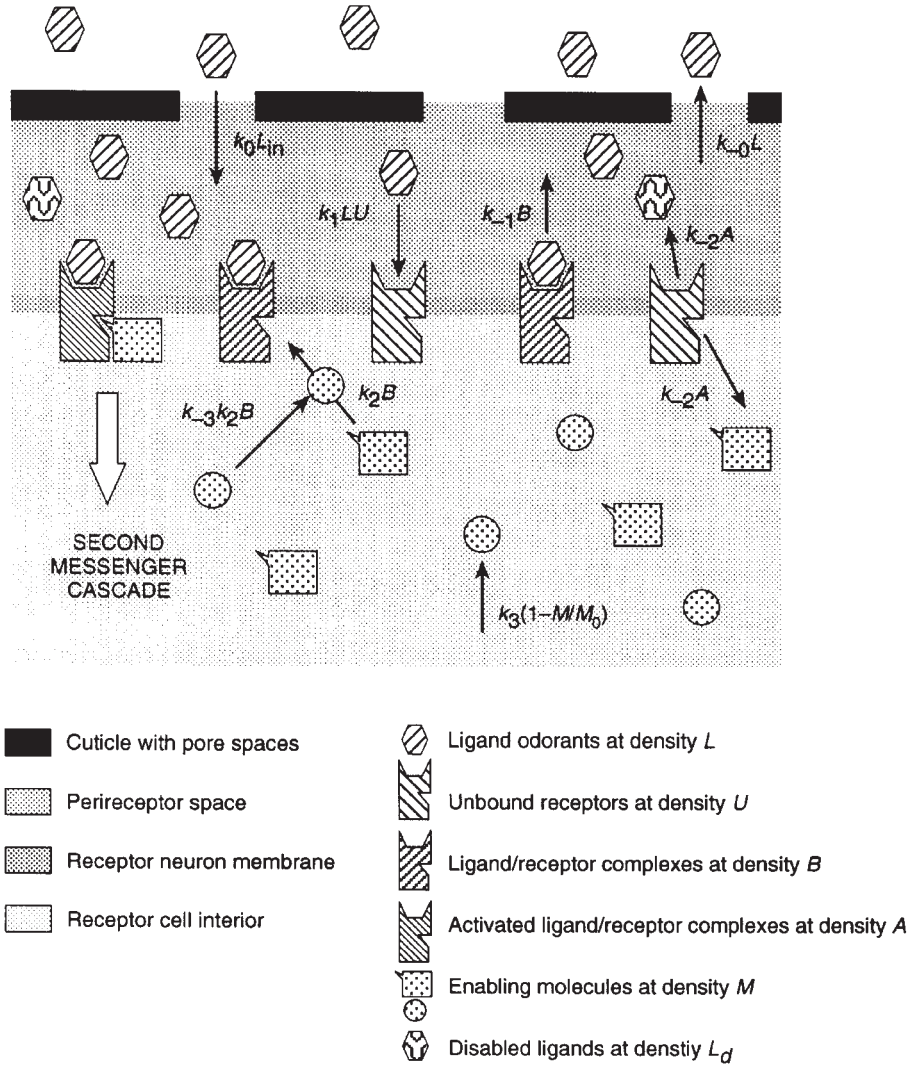

Figure 1 A diagram of an ORN and the primary dynamic processes used to model the density A of activated ligand–receptor complexes (densely hatched ligand and receptor molecules bound with checkered enabling molecules), which are then linked directly in the model to changes in membrane potential (cf. equation 6). Equations (1)–(5) describing this process involve the ligand flux input L_{in} into perireceptor space, unbound ligand density variable L, unbound receptor density variable U, bound ligand–receptor complex density variable B, enabling molecule density variable M (an aggregation of G-proteins, ATP molecules, etc.—see text) and its background level M_0. The parameters k_0 and k_i, $i = \pm 1, \pm 2, \pm 3$, are associated rate constants (see text for more details).

receptors at density B become activated receptors at density A is typically modeled by the simple kinetic process

$$B \underset{k_{-2}}{\overset{k_2}{\rightleftarrows}} A$$

(Lánsky and Rospars, 1999). One can assume also that the ligands themselves enter the perireceptor space at a rate determined by an externally determined flux density $k_0 L_{in}$ (L_{in} is a density and k_0 is a rate) and leave at the same per-capita (i.e. per molecule) rate they enter. Further, one can assume, as in Lánsky and Rospars (Lánsky and Rospars, 1999), that the ligands become inactivated during the dissociation process

$$B \xrightarrow{k_{-1}} U + L_d$$

where L_d is the density of degraded ligands that are no longer able to play a role in generating a response. Recent evidence, however, suggests that termination of olfactory signaling has more to do with direct deactivation of ligand–receptor–G-protein complexes, than ligand degradation *per se* (Breer, 1994). For want of specifics regarding the mechanisms of receptor inactivation, I assume that the activated ligand–receptor–G-protein complexes are inactivated at a per-unit rate k_{-2}, leaving behind, after a sequence of reactions much faster than k_{-2}, an intact unbound receptor and a degraded ligand (Figure 1). Thus the inactivation processes can be approximated by the dissociation process

$$A \xrightarrow{k_{-2}} U + L_d$$

leading to equations (1)–(3) in the Appendix.

To model the activation process in a more realistic manner, one may need to take account of the fact that the activation processes require the presence of resources in the form of ATP, G-proteins, Ca^{2+} (Restrepo *et al.*, 1996) and other molecules on which the activation rate k_2 depends (Figure 1). One might expect the activation rate k_2 to decline with decreases in the density M of these second-messenger-related molecules, which here I generically refer to as 'enabling molecules'. Thus, at high densities of L, if the complex B is produced rapidly, then the activation process may become partially exhausted through a reduction in the density M, although M will probably not decline to zero. The reason for this is because these enabling molecules, at density M, are maintained by cellular processes that replenish or recycle the molecules involved in the activation processes and restore the density of these molecules to a resting level M_0 during a refractory period after the ligand input density L_{in} becomes zero [in reality, ligand input density is a function of time $L_{in}(t)$].

In the absence of specific details, one might expect the activation rate k_2 to be an increasing function of the ratio of the density M of activation enabling molecules to the density B of bound receptors, i.e. $k_2 = k_2(M/B)$. One would expect this function to saturate at some maximal rate k_2^* when (i.e. when enabling molecules are not limiting). A simple function with this saturating property is the Monod function, where the onset of saturation is controlled by its associated Michaelis–Menten 'half-saturation' parameter $M_{1/2}$—see equation (4) in Appendix A; for a review of this function see Smith and Waltman (Smith and Waltman, 1995). If the density M of these enabling molecules is drawn down at a rate proportional to the activation process rate k_2B, while simultaneously being restored by cellular processes to a resting density M_0, then the kinetics of M is modeled by equation (5) in the Appendix.

Modeling neuron spike rates

The relationship between the density of activated ligand–receptor complexes and the spike rate of an olfactory neuron is complicated by the second messenger cascade that ultimately results in the opening of the ion channels that lead to the production of spikes. Without the details of all, or even the major, biochemical pathways involved in this second messenger cascade, I need to make some simplifying assumptions regarding the relationship in questions. First, I assume that the adaptive processes going on in the cell are captured by the notion of enabling molecules and the saturating kinetic relationship expressed in equation (4). Second, I explicitly model the voltage dynamics of the receptor neuron membrane and then make the standard assumption that spike rate is some appropriate function of membrane voltage (Rospars *et al.*, 1996).

Consider a membrane voltage depolarization and resting state restoration model based on the simple assumption that competing restorative and depolarizing forces are proportional to differences in membrane voltage respectively with regards to resting (V_{rest}) and maximum depolarizing (V_{dep}) levels (note $V_{rest} < V_{dep}$). Also, assume that the rate of membrane depolarization is proportional to the density of activated ligand–receptor complexes $A(t)$. Under these assumptions, changes in membrane voltage $V(t)$ are modeled by the equation (6) in the Appendix. Further, if it is now assumed that the maximum spike rate for a neuron is S_{max}, and that a neuron will not spike if $V(t) < V_{crit}$, then the simplest model for the instantaneous spike rate incorporating this threshold is a clipped linear time-delay model scaled by the maximum spiking rate with changes in voltage normalized by the maximum possible change maximum equal to ($V_{dep} - V_{crit}$)—see equation (7) in the Appendix.

It is not directly possible to measure an instantaneous spike rate, only an average spike rate $\overline{S}(t_1,t_2)$ over an arbitrary time interval $[t_1,t_2]$ or, of course, interspike intervals [equation (8) in Appendix]. Here, to be compatible with data used to fit the model, we compute the average spike rates over consecutive 50 ms time bins.

Results

Baseline dynamics

I first set out to explore the dynamics of the ligand–receptor binding and activation process, modeled by equations (1)–(5) in the Appendix. These equations constitute a fourth-order nonlinear system of ordinary differential equations in the 'ligand', 'ligand–receptor', 'activated ligand–receptor' and 'enabling molecules' density variables L, B, A and M, respectively. These equations contain seven rate parameters (k_0, k_1, k_{-1}, k_2^*, k_{-2}, k_3 and k_{-3}), an input parameter or, more generally, function of time $L_{in}(t)$, three density scaling parameters, R, $M_{1/2}$ and M_0, and, of course, four initial conditions, $L(0)$, $B(0)$, $A(0)$ and $M(0)$. Without loss of generality, I scaled the units of all parameters with respect to the total number of receptor molecules $R = U(t) + A(t) + B(t)$ per unit receptor neuron membrane. Note that we have assumed R to be constant over time, even though the relative densities of receptors in the different states $A(t)$ and $B(t)$ change with time. To implement this scaling, we set $R = 1$ and interpret the other densities in terms of R; for example, $L_{in} = 0.1$ means that the ligand density in the perireceptor space is 1/10th the density of the total receptor molecule density R. Without loss of generality, we can also scale time. For notational simplicity, the variable we choose as our basic unit of time is $k_2^* = 1$, the maximum rate at which ligand–receptor complexes are activated [which only occurs when densities of $M(t)$ are much greater than $M_{1/2}B$—see expression (4)].

The model is capable of producing a complex array of output patterns for different values of the rate and scaling

parameters, as well as initial conditions. One way of investigating the effects of these parameters and initial conditions is by systematically studying several simpler special cases and the sensitivity of solution output to these special cases. The particular cases selected here are motivated by the need both to understand the range of possible patterns (analysis of contrasting cases) and to search for output patterns that resemble empirical data. In particular, it would be useful to obtain an understanding of how certain processes influence the temporal profiles of the response of receptors to constant, as well as pulsatile, stimuli.

To begin, I conducted a baseline analysis for the simplified case $k_0 \to \infty$, $k_{-1} = 0$, $k_1 = 1$, $k_{-2} = 1$, $k_3 = 1$, $k_{-3} = 1$ and $L_{in}(t) = 1$ for all $t \geq 0$ (recall $k_2^* = 1$ and $R = 1$), by first numerically simulating the behavior of the solution to equations (1)–(5) when the density scaling parameters have the values $M_{1/2} = 1$ and $M_0 = 1$ (Figure 2A–D), or $M_0 = 10$ (Figure 2E–H). The initial conditions used are the resting values of the system (i.e. the equilibrium state of the system in the absence of any external stimuli); i.e. $B(0) = 0$, $A(0) = 0$, and $M(0) = M_0$. I then considered the effects of altering the rate parameters k_1, k_{-2}, k_3 and k_{-3} with respect to the basal simulations of the equations over the interval $t \in [0,20]$. Note that letting $k_0 \to \infty$ in equation (1) is equivalent to assuming that at all times, the actual density $L(t)$ is equal to the input density $L_{in}(t)$. Relaxing this assumption basically sets up a time lag, inversely related to the size of the rate constant k_0, in which the ligand density follows the input $L_{in}(t)$ at a distance that depends on how rapidly ligands bind to available receptors. The dynamics would be a little more complicated than just a pure time lag, however, and the ORNs would then take on features associated with flux detectors, rather than concentration detectors, as discussed by Kaissling (Kaissling, 1998a).

The results indicate (Figure 2A,E) that the rate k_1 at which ligand and receptor molecules associate serves to scale the equilibrium proportion of activated ligand–receptor complexes up to a saturating proportion (the value for very large k_1) of ~0.35 when $M_0 = 1$ (Figure 2A) and 0.5 when $M_0 = 10$ (Figure 2E), given that the other rate parameters are unity. On the other hand, the parameter k_1 influences the shape of the transient rather than the equilibrium value when the enabling molecule density recovery rate is a relatively slow $k_3 = 1/30$ (Figure 3A). The rate k_{-2} at which activated ligand–receptor complexes dissociate into available unbound receptors and the density L_d of disabled ligands has an inverse effect on the ligand–receptor complex equilibrium proportion, both when $k_3 = 1$ (Figure 2B,F) and $k_3 = 1/30$ (Figure 3B). The enabling molecule recovery rate k_3 produces a strong peak-shaped ligand–receptor activation profile when the other parameters have the basal values of unity, but then only when it has a sufficiently small (i.e. slow) value itself (Figure 3C). This peak disappears when the enabling molecule resting density is increased by an order of magnitude to $M_0 = 10$ (Figure 3G) and the transient become

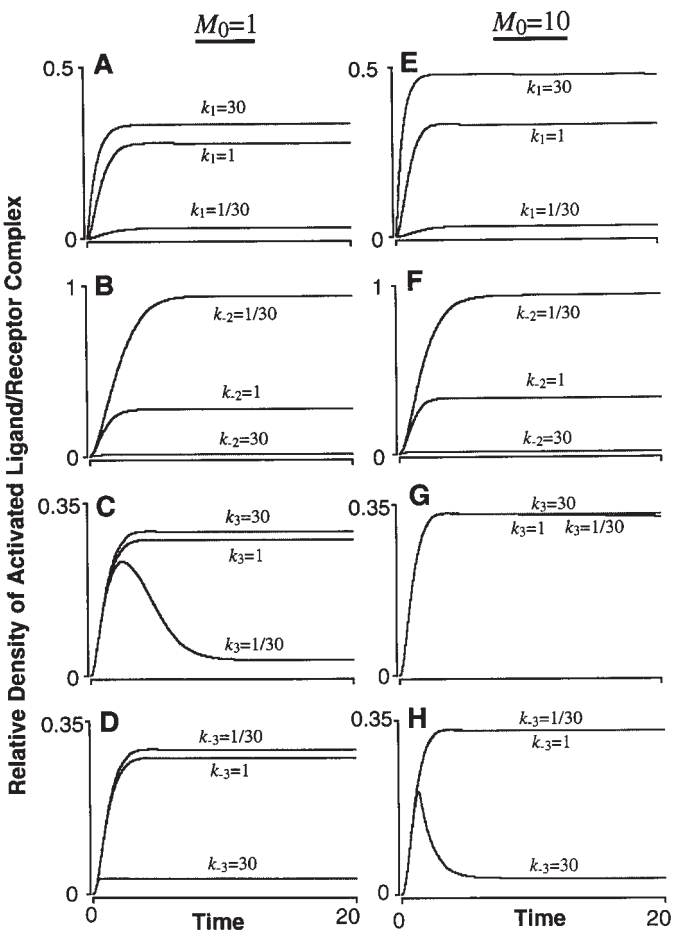

Figure 2 Numerical solutions to equations (1)–(5) for the variable $A(t)$ (density of activated ligand–receptor complexes) are plotted over 20 units of time (1 unit = 200 ms) for the baseline parameter values $k_0 \to \infty$ [i.e. equation (1) falls away and $L(t)$ $L_{in}(t)$), $k_{-1} = 0$, $k_2^* = 1$, $R = 1$, $L_{in}(t) = 1$, $M_{1/2} = 1$, $M_0 = 1$ (**A**–**D**) or $M_0 = 10$ (**E**–**H**) and, unless otherwise indicated in A–D and E–F, $k_1 = 1$, $k_{-2} = 1$, $k_3 = 1$, $k_{-3} = 1$. The initial conditions for all eight solutions are $A(0) = 0$, $B(0) = 0$ and $M(0) = M_0$.

insensitive to the enabling molecule recovery rate k_3. The rate k_{-3} at which at which the enabling molecules are used up when activating ligand–receptor complexes also has an increasing effect on the ligand–receptor complex equilibrium proportion, both when $k_3 = 1$ (Figure 2D) and $k_3 = 1/30$ (Figure 3C). At the higher resting density of ten enabling units per receptor ($M_0 = 10$), the equilibrium proportion of activated ligand–receptor complexes hardly increases for corresponding values of the various rate parameters, although a strong peak arises when the rate k_{-3} increases to 30 (Figure 2H) or even when k_{-3} is only equal to 1 for the case $k_3 = 1/30$ (Figure 3C).

Fitting real receptor neuron spike profiles

Empirical data from both the honey bee *Apis mellifera* (Akers and Getz, 1992, 1993; Getz and Akers, 1993) and the American cockroach *Periplaneta americana* (Lemon and

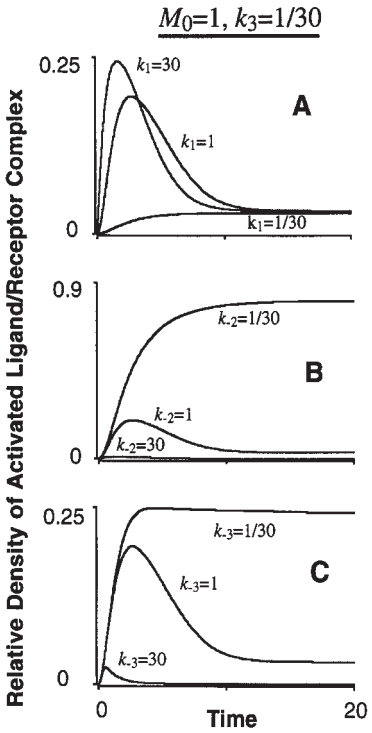

Figure 3 Numerical solutions to equations (1)–(5) for the variable $A(t)$ (density of activated ligand–receptor complexes) are plotted over 20 units of time (1 unit = 200 ms) to investigate the case when the enabling molecule density $M(t)$ recovery rate is the relatively slow value k_3=1/30. The remaining parameters have the baseline parameter values $k_0 \to \infty$, $k_{-1} = 0$, $k_2^* = 1$, $R = 1$, $L_{in}(t) = 1$, $M_{1/2} = 1$, $M_0 = 1$ and, unless otherwise indicated, $k_1 = 1$, $k_{-2} = 1$, $k_{-3} = 1$. The initial conditions for all three solutions are $A(0) = 0$, $B(0) = 0$ and $M(0) = M_0$.

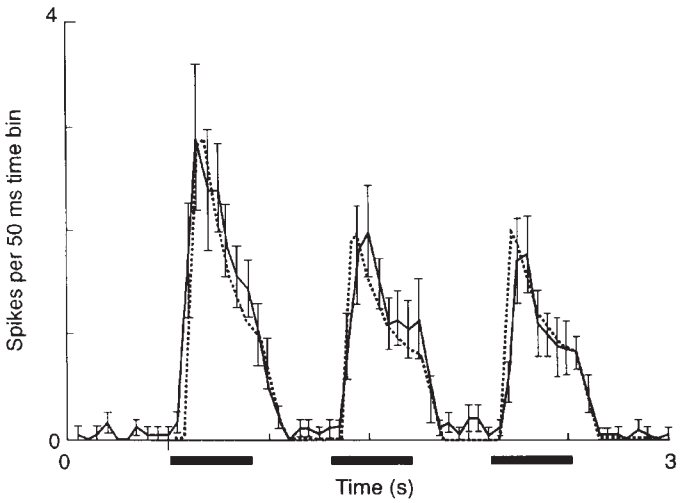

Figure 4 The average spike rate $\bar{S}(t_1,t_2)$ (see equation 8) was calculated over consecutive 50 ms intervals of time (because 1 unit of time is 200 ms, we have $[t_1,t_2]$ = [0,0.25], [0.25,0.5], … ,[14.75,15]) from a numerical solution of equations (1)–(6) and (10) for the input flux L_{in} equal to a pulsed 1.25 Hz square-wave (solid bars below abscissa) of height 5 units (i.e. five times the density of the molecular receptors in all possible states), using the parameter values $k_1 = 5$, $k_{-1} = 100$, $k_{-2} = 2$, $k_3 = 100$, $k_{-3} = 3.5$, $M_{1/2} = 0.1$, $M_0 = 10$, $a_0 = 10$, $a_1 = 80$, $V_{crit} = -45$ mV, $V_{rest} = -50$ mV, $V_{dep} = +50$ mV, $t = 0.1$, and $S_{max} = 200$, as well as the initial conditions $A(0) = 0$, $B(0) = 0$, $M(0) = M_0$ and V(0) = –50 mV. The results are plotted as an overlay (grey line from the 0.5 s mark to the 3 s mark) to an empirical data set (represented by the solid line with associated error bars) obtained from recording the responses of a population of cockroach ORNs to a 1-hexanol stimulus pulsed at the same 1.25 Hz frequency (Lemon and Getz, 1997).

Getz, 1997) indicate that the average firing rate of a population of olfactory receptor neurons has a peak-shaped profile similar to that displayed in Fig 3A for the cases k_1 = 1 and k_1 = 30.

These data were obtained from recording the responses of a population of cockroach ORNs to a pulsed 1.25 Hz square-wave 1-hexanol stimulus (Lemon and Getz, 1997). The means and standard errors of these data (N = 20 receptors in the data set) are illustrated in Figure 4.

Equations (1)–(7) can be used to simulate the data in Figure 4. These seven equations contain one input function $L_{in}(t)$ and 17 adjustable parameters (R, k_0, k_1, k_{-1}, k_2^*, k_{-2}, k_3, k_{-3}, $M_{1/2}$, M_0, a_0, a_1, V_{rest}, V_{dep}, V_{crit}, S_{max} and t). Two of these parameters can be set to unity to scale the equations to relative units of time and density. Thus I set $k_2^* = 1$ and $R = 1$. Also, as previously mentioned, I let $k_0 \to \infty$ which allows the ligand density to be replaced with an input function $L_{in}(t)$ (note that I made this assumption more realistic by imposing a 20 ms time delay on this function). The remaining 14 parameters represent a large number of degrees of freedom for fitting the output of a model to the given data. I thus reduced the number of free parameters by further setting V_{rest} = –50 mV, which is within 10 mV of the resting potential of many cockroach neurons (Burrows, 1996). I set V_{dep} = +50 mV, which is close to the Nernst potential (i.e. the potential at which a particular ion stops flowing across the membrane) generated by the fast Na^+ depolarizing current in the giant squid axon (Koester, 1991). I set the maximum spike rate to S_{max} = 200 spikes/s based on the fact that the width of a spike in an insect olfactory neuron is ~3–4 ms (Akers and Getz, 1992). I scaled time so that 1 unit of time represents 200 ms. This implies that the input function $L_{in}(t)$ switches on and off every two units of time.

An informal search over the remaining parameter space produced the following set of parameters that provided an excellent fit to the empirical data (Figure 4): k_1 = 5, k_{-1} = 100, k_{-2} = 2, k_3 = 100, k_{-3} = 3.5, $M_{1/2}$ = 0.1, M_0 = 10, a_0 = 10, a_1 = 80, V_{crit} = –45 and t = 0.1 (i.e. 20 ms).

From visual inspection, these parameters provide a good fit. Of course, a better fit could be obtained using least-squared or maximum-likelihood methods (Hilborn and Mangel, 1997). This level of precision, however, would only be justified if more scenarios were used to make the fitting procedure more robust (for example, several different concentrations, input waveforms, etc.), an exercise beyond the scope of this paper and the available data.

Finally, additional simulations were undertaken to

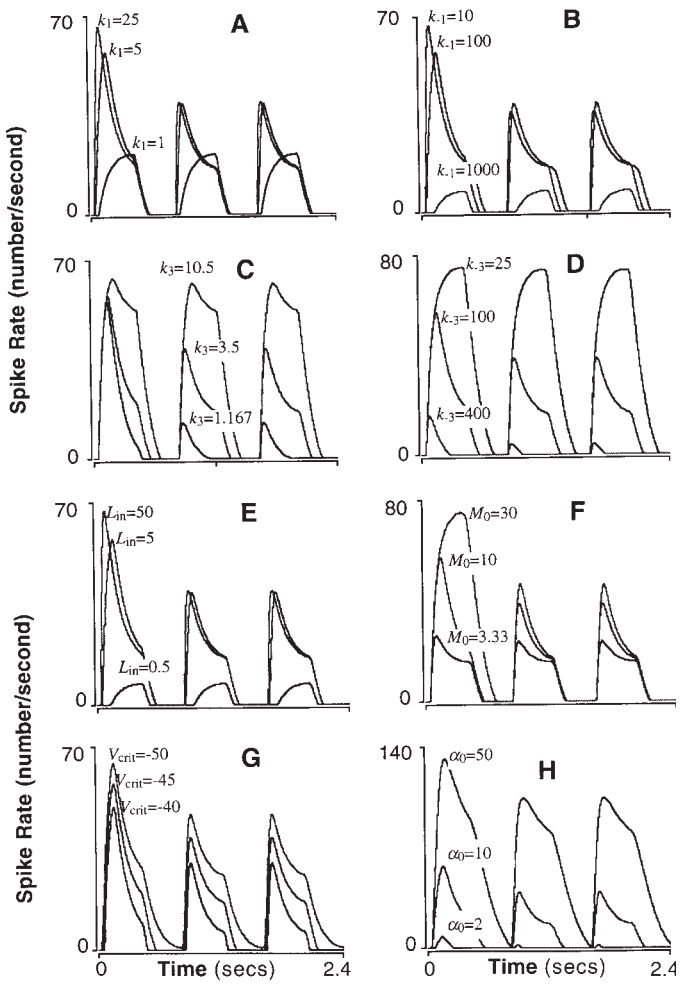

Figure 5 Simulated spike rates are generated from for model for the parameter values listed in Figure 4, except for changes to the values specifically indicated in each of the three trajectories plotted in panels **A**–**H**.

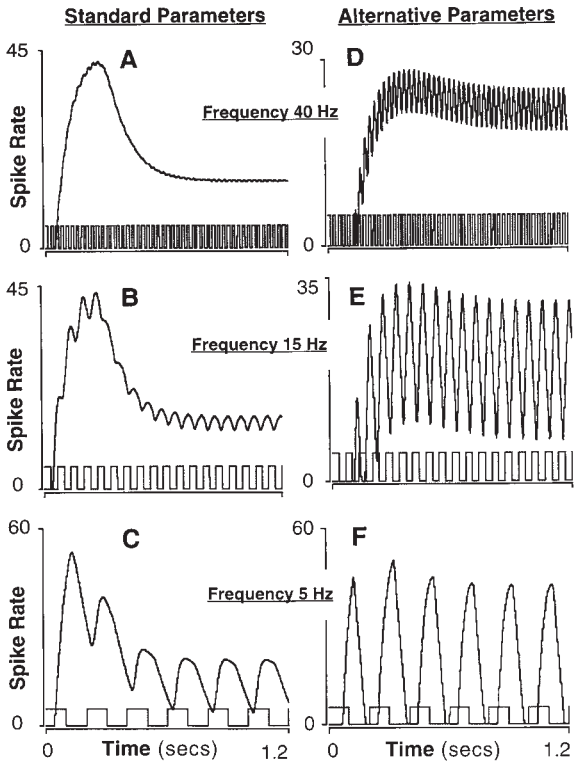

Figure 6 The spike rates of two neurons—one bearing the standard parameters listed in Figure 4 and the second bearing the same parameters except for the changes $k_{-3} = 10$, $a_0 = 50$, $a_1 = 1000$ and $V_{crit} = -10$ (alternative parameters)—are plotted for the cases where the ligand input $L_{in}(t)$ are pulses of square waves of amplitude 2 (plotted below the trajectories) at the labeled frequencies. As discussed more fully in the text, the alternative set of parameters produces a neuron that is able to follow high frequency inputs much faster than a standard neuron.

explore the sensitivity of different features in the spike rate profile (for example, existence of a prominent peak, shape of peak, on- and off-set characteristics; Figure 5) and the ability of the spike train to follow a pulsed stimulus (Figure 6). The implications of these results are discussed below.

Discussion

Relationship among parameters

The primary purpose of this paper is to present the model and investigate how well the processes incorporated in the model are able to reproduce empirically measured output, because the model will then be used to generate input into a neural network model of the insect antennal lobes (Getz and Lutz, 1999). If the model fits a limited data set well, then one can move to collecting a more demanding set of data (more concentrations, a greater variety of stimulus patterns, etc.) on which to test the model and refine or extend it. Further, in testing a model, one's confidence in how well the model captures the essential processes increases with the number of parameters that are independently estimated; for example, direct measurement of V_{rest}, V_{dep} and V_{crit}, and of as many of the rate constants and component densities as possible (Kaissling, 1998b). Thus, the ultimate test of the model is to see how well it reproduces the output for a variety of stimuli when all of the model parameters are estimated independently of the output.

Given the paucity of suitable data, I was unable to estimate (i.e. fix) values for the majority of the parameters before selecting the values for the remaining set. Further, the model certainly omits the details of many processes contributing to the production of ORN spike trains in response to a given stimulus. Even so, the model still has considerable value in generating hypotheses regarding relationships among the rate constants of the identified processes, and then testing these to see how well they stand up to scrutiny in real systems.

For example, in trying to find a set of parameters that provide an approximate fit to the data, it is clear from

Figures 2 and 3, especially Figure 3A, that one needs to select a set of parameters for which $k_1 << 1$ and $k_3 >> 1$. From a visual inspection of the fit between model output and empirical data (Figure 4), it is apparent that the model captures well the reduction in the second and third peaks of the data compared with the first peak. The model also captures the fast rise in the first peak, but clearly shows that the data indicate a slower rising second peak and an even slower rising third peak that could be due to relatively slow adaptive processes not accounted for in the model. Several important points emerge from a comparative study of how the spike rate changes with the relative values of the parameters used to fit the model (Figure 5).

First, a relatively large (fast) ligand–receptor binding rate, k_1, is needed to keep the the observed peak (Figure 4) sharp. For example, if we drop the value of k_1 by a factor of five to $k_1 = 1$, no adaptation (i.e. presence of a peak) is evident: the response is cut off at its maximum value by the off-set of the stimulus (Figure 5A). On the other hand, once k_1 is sufficiently large, increasing its value by a factor of five to $k_1 = 25$ has a relatively small effect on the shape of the peak (Figure 5A).

Second, the ligand–receptor dissociation rate, k_{-1}, can be relatively large (fast) compared with the ligand–receptor binding rate k_1, and the transient peak still retained, but not too large to prevent significant ligand–receptor activation and initiation of a dense second messenger cascade (Figure 5B). On the other hand, k_{-1} should not be too small (slow), since this leads to a slower decay of spike activity once the stimulus has been removed (Figure 5B).

Third, generation of a strong peak requires the rate k_3 at which enabling molecules catalyze the activity of bound receptor/ligand complexes to be considerably faster than the enabling molecule cellular restoration rate k_{-3} (cf. Figure 2C with $k_3 = 1/30$ and Figure 2H with $k_{-3} = 30$). This difference causes enabling molecules to become limiting and adaptation to set in, provided the absolute values of the rates k_3 and k_{-3} are appropriately scaled with respect to the resting enabling molecule density M_0 and the ligand input density L_{in} (compare Figure 2C with 2G and Figure 2D with 2H). Further, when the input ligand density is pulsed, if k_3 is decreased to the point where it is almost two orders of magnitude smaller (slower) than k_{-3}, then the height of the first peak is hardly affected, but the second and third peaks are now a fraction of the height of the first peak (Figure 5C). By contrast, the second and third peaks become much closer to the height of the first peak if either k_3 is increased or k_{-3} is decreased (Figure 5C,D).

Fourth, the peaked behavior is not evident unless the ligand input and/or the enabling molecule resting concentrations, L_{in} and M_0 respectively, are sufficiently high (Figure 5E,F). These results, together with the above results, imply that the existence of a transient peak is dependent on the relative relationship of the densities of the variables (ligands, free receptors, enabling molecules) to the values of the rate parameters. Therefore, the absolute values of the rate parameters can only be set by measuring the true densities of the variables involved or vice versa. Note that the half saturation parameter $M_{1/2}$ has little effect on the shape of the curve for the set of parameters considered here, so the results have not been included in Figure 5.

Fifth, the parameter V_{crit}, as expected, affects the absolute height of the peak but, more importantly, it is critical in determining the offset characteristics of the spike train. If the critical voltage at which the cell begins its spike activity, V_{crit}, equals the resting voltage V_{rest} (= –50 mV), then the spike activity follows the process of the restoration of the voltage to its resting state so that the relatively sharp switch of the neuron to its off position is lost (Figure 5G). On the other hand, since our model is deterministic, no background spike rate is possible when the neuron is switched off. The low background spiking level evident in the empirical data can easily be incorporated into the model by including an appropriate low noise level in the spike generation process.

Finally, the voltage parameters a_0 and a_1 need to be relatively large for the spike train to reproduce (or follow) steep inclines and declines, as well as sharp peaks, that occur in the density of the activated ligand–receptor complexes (cf. Figures 2 and 3). These peaks, however, will not be effectively followed unless the voltage depolarizing parameter a_1 is larger than the voltage restoration parameter a_0 (Figure 5H). Further, the larger this discrepancy, the more easily the receptor is able to rise to its maximum spike frequency of $S_{max} = 200$ Hz.

Pulsatile stimuli

Empirical data indicate that odor stimuli often take the form of turbulent odor plumes containing discrete packets of odor. Thus, as an insect flies through or along an odor plume or an odor plume is transported over a stationary insect, the packets of odor are perceived as a sequence of pulses of varying pulse and inter-pulse duration (Murlis *et al.*, 1992; Vickers and Baker, 1994). If the inter-pulse intervals are short compared with the constants characterizing the response of the ORNs, we can expect the ORNs to smooth out the pulses, while if the inter-pulse intervals are relatively large, then each pulse should be transparent to the system (Lemon and Getz, 1997). By comparing model output to empirical data on the response of ORNs to pulsatile stimuli, one can test whether the time constants in the model are compatible with observed data. The simulation results presented in Figure 6 provide some insight into how model output changes for changes in selected rate constants.

The specific set of ORN parameters used to fit the cockroach data presented in Figure 4 smooth out pulsatile square wave stimuli of amplitude 2 oscillating at frequencies of 40 Hz or higher (Figure 6A). Once these pulsatile stimuli have dropped to frequencies of ~15 Hz, the oscillations are evident in the simulations (Figure 6B), although in real

ORNs noise may mask these oscillations in individual response profiles. At frequencies of ~5 Hz (Figure 6C), the oscillations are strongly evident and unlikely to be masked by noise, even in individual ORNs.

Real populations of cockroach olfactory receptor neurons appear to be able to follow to some extent oscillations of 20 Hz and even 40 Hz (Lemon and Getz, 1997). One of the reason our simulated receptors are not able to follow frequencies much higher than 10 Hz is in part due to the fact that the offset response (at the end of each square wave) is too slow. The offset response rate can be increased by decreasing the value of V_{crit}. This, however, would lead to a significant decrease in the spike rate (Figure 5G), which can be compensated by reducing the value of k_{-3} and the ratio of a_0 to a_1. Further the absolute values of both these parameters can be increased so that the voltage can more accurately follow changes in the densitiy of the activated ligand–receptor complexes. Responses of ORNs modeled by equations (1)–(6), using the standard parameter set used to generate Figure 6A–C, with the modifications $k_{-3} = 10$, $a_0 = 50$, $a_1 = 1000$ and $V_{crit} = -10$, produces output that clearly follow 4 and 15 Hz pulses (Figure 6E,F). Populations of these ORNs would even follow 40 Hz pulses in populations of neurons if the signal-to-noise ratio were not too large (Figure 6D).

Synergism and inhibition

Many insects and crustacean chemosensory receptors exhibit synergistic or inhibitory characteristics when responding to mixtures of several odorants or stimulants (Daniel and Derby, 1988, 1991a, 1991b; Derby *et al*., 1991; Fine-Levy and Derby, 1992; Getz and Akers, 1995). Inhibition is particularly widespread in arthropods and is thought to be associated with IP_s second messenger pathways (Ache and Zhainazarov, 1995; Daniel *et al*., 1996). The phenomena of synergism and inhibitions have been defined in several different ways, some more useful than others (Getz and Akers, 1995).

Interactions between odorants in generating a response rate S in an olfactory receptor neuron can occur at several different levels. First, two ligands may compete directly for binding sites on the same receptor molecules. Second, different ligands may bind with different receptor molecules on the dendritic membrane of the same receptor neuron and these bound ligand–receptor complexes may be activated by the same set of enabling molecules; third, by a partially overlapping set of enabling molecules; or, fourth, by a non-overlapping set of enabling molecules. Fifth, even if two different ligands initiate distinct second messenger cascades, the final products of these cascades may open the same ion channels or, sixth, different ion channels in the receptor cell membrane.

In the last case, one ligand may lead to depolarization and the other to hyperpolarization of the receptor neuron membrane. The voltage model developed here is easily extended to include hyperpolarizing pathways. Specifically, the depolarizing and hyperpolarizing pathways can each be modeled by a set of equations [equations (1)–(5) in the Appendix] with variables and parameters subscripted (or double subscripted if already subscripted) to indicate the pathway in question. Thus, in this case, for $i = 1, 2$, we can have $A_i(L_i,t)$ representing the density of activated ligand–receptor complex at time t when the density of ligands i in the perireceptor space has the time profile $L_i(t) = L_i$. If we now assume that depolarizing, restorative and hyperpolarizing ionic channel and pump processes compete to drive the voltage to the respective levels $V_{dep} > V_{rest} > V_{hyp}$ (note that the resting membrane potential V_{rest} is negative in neurons) at rates that are proportional to the voltage gradients involved and, additionally, the depolarizing and hyperpolarizing rates are respectively proportional to the densities of the activated ligand–receptor complexes $A_1(L_1,t)$ and $A_2(L_2,t)$, then the membrane voltage [equation (6)] can be extended to include both pathways [equation (9) in the Appendix]. Unfortunately, no appropriate data exist to explore how well this extension is able to simulate the response of olfactory receptor cells containing both types of pathways, so a test of the extended model remains a tantalizing opportunity for future studies.

Finally, from an olfactory coding perspective, it may be more important for the model to fit data over some parts of the response profile than others. For example, honey bee ORN data (Getz and Akers, 1992), which exhibit peak response rates occurring, as with the cockroach, during the interval 50–150 ms after the onset of each stimulus (Figure 4), appear to code more information during this peak response period than during post-peak period of 150–250ms (Getz and Akers, 1997b). If this situation also applies to cockroach ORN data, then it is more critical that the model fits the data over the interval 50–150 ms after the onset of a stimulus than over time intervals much beyond this particular window of time.

Conclusion

Chemical signaling processes based on G-protein associated receptor transduction mechanisms incorporate complex second messenger cascades involving many tens of interactions and synthesis of intermediate products, not to mention links to more general cellular processes involving the cycling of such energy resources as ATP, and all-purpose messenger molecules such as cAMP and Ca^{2+}. A precise model for the generation of membrane voltage profiles, and hence spiking behavior, of ORNs would require that all the essential details of the associated second messenger cascades be known. Thus a precise model is not yet feasible, since many details remain to be worked out. Further, as long as a complete description of all cellular processes competing for critical energy and messenger molecules is not included in the model, simplifying assumptions need to be made

to obtain workable models of the response of ORNs to stimulation. These assumptions may be reasonable if the processes modeled by equations are orders of magnitude faster or larger than those subsumed under postulates of constant background levels, constant fluxes, or phenomenologically specified relationships, such as the one postulated in equation (4).

Most ORN response models in the literature have been either been applicable to cells that respond to single odorants (such as pheromone receptors in insects), or to general olfactory cells stimulated by odorants rather than complex odor stimuli. Some models do consider stimulation by complex odor stimuli but, as in Malaka *et al*. (Malaka *et al*., 1995), they only consider the equilibrium situation, they do not model the membrane voltage and they do not consider nonlinearities arising from the ligand–receptor activation process being limited by ATP, G-proteins, or other enabling molecules ([f. equation (4)]. Also, many studies focus on the equilibrium (tonic) rather than transitory (phasic) properties of response neurons (Rospars *et al*., 1996), despite the fact that the phasic response in general olfactory receptors in insects lasts at least 200 ms (Lemon and Getz, 1997). This phasic period is not much shorter than the time it takes worker honey bees, for example, to discriminate different odors (Smith and Menzel, 1989).

Although many details of the pathway involved in transducing olfactory signals into electrical responses in insect and other animal olfactory sensory neurons are not known, and a number of simplifying assumptions were made in developing the model presented here, the model captures exceptionally well the spike rate of cockroach olfactory neurons to pulsatile odors. More detailed empirical data on the response of neurons to pure and mixed odor stimuli with various concentration profiles (for example, both square and triangular shaped pulses) are required to provide a richer array of patterns for fitting the model. Also, more details on the various transduction pathways are needed before we can assess how well a nonlinear relationship, such as portrayed in equation (4), is really able to encapsulate the complex array of processes associated with signal transduction by ORNs.

Acknowledgements

I thank William Lemon, Petr Lánsky and Jean-Pierre Rospars for comments on the manuscript. This work was support by NSF Grant IBN 98-07938 to W.M.G.

References

Ache, B.W. (1994) *Towards a common strategy for transducing olfactory information*. Cell Biol., 5, 55–63.

Ache, B. W. and **Zhainazarov, A.** (1995) *Dual second-messenger pathways in olfactory transduction*. Curr. Opin. Neurobiol., 5, 461–466.

Akers, R.P. and **Getz, W.M.** (1992) *A test of identified response classes among olfactory receptors in the honeybee worker*. Chem. Senses, 17, 191–209.

Akers, R.P. and **Getz, W.M.** (1993) *Response of olfactory sensory neurons in honey bees to odorants and their binary mixtures*. J. Comp. Physiol., 173, 169–185.

Boeckh, J., Distler, P., Ernst, K.D., Hösl, M. and **Malun, D.**(1990) *Olfactory bulb and antennal lobe*. In Schild, D. (ed.), Chemosensory Information Processing. Springer, Berlin, pp. 201–227.

Breer, H. (1994) *Odor recognition and second messenger signaling in olfactory receptor neurons*. Cell Biol., 5, 25–32.

Buck, L. and **Axel, R.** (1991) *A novel multigene family may encode odorant receptors: a molecular basis for odor recognition*. Cell, 65, 175–187.

Burrows, M. (1996) The Neurobiology of an Insect Brain. Oxford University Press, New York, pp. 682.

Daniel, P.C. and **Derby, C.D.** (1988) *Behavioral olfactory discrimination of mixtures in the spiny lobster (*Panulirus argus*) based on a habituation paradigm*. Chem. Senses, 13, 385–395.

Daniel, P.C. and **Derby, C.D.** (1991a) *Chemosensory responses to mixtures: a model based on compostion of receptor cell types*. Physiol. Behav., 49, 581–589.

Daniel, P.C. and **Derby, C.D.** (1991b) *Mixture suppression in behavior: the antennular flick response in the spiny lobster towards binary odorant mixtures*. Physiol. Behav., 49, 591–601.

Daniel, P.C., Burgess, M.F. and **Derby, C.D.** (1996) *Responses of olfactory receptor neurons in the spiny lobster to binary mixtures are predictable using a noncompetitive model that incorporates excitatory and inhibitory transduction pathways*. J. Comp. Physiol A., 178, 523–536.

Derby, C.D., Girardot, M. and **Daniel, P.C.** (1991) *Responses of olfactory receptor cells of spiny lobsters to binary mixtures. II. Pattern mixture interactions*. J. Neurophysiol., 66, 131–139.

Dittmer, K., Grasso, F. and **Atema, J.** (1995) *Effects of varying plume turbulence on temporal concentration signals available to orienting lobsters*. Biol. Bull., 189, 232–233.

Ennis, D.M. (1989) *A receptor model for binary mixtures applied to the sweetness of fructose and glucose: De Graaf and Frijters revisited*. Chem. Senses, 14, 597–604.

Ennis, D.M. (1991) *Molecular mixture models based on competitive and non-competitive agonism*. Chem. Senses, 16, 1–17.

Fine-Levy, J.B. and **Derby, C.D.** (1992) *Behavioral discrimination of binary mixtures and their components: effects of mixture interactions on coding of stimulus intensity and quality*. Chem. Senses, 17, 307–323.

Firestein, S. and **Shepherd, G.M.** (1991) *A kinetic model of the odor response in single olfactory receptor neurons*. J. Steroid Biochem. Mol. Biol., 39, 615–620.

Firestein, S. and **Zufall, F.** (1994) *The cyclic nucleotide gated channel of olfactory receptor neurons*. Cell Biol., 5, 39–46.

Fujimura, K., Yokohari, F. and **Tateda, H.** (1991) *Classification of antennal olfactory receptors of the cockroach,* Periplaneta americana *L*. Zool. Sci., 8, 243–255.

Getz, W.M. (1993) *Metaphysiological and evolutionary dynamics of populations exploiting constant and interactive resources: r–K selection revisited*. Evol. Ecol., 7, 287–305.

Getz, W.M. and **Akers, R.P.** (1993) *Olfactory response characteristics and tuning structure of placodes in the honey bee* Apis mellifera *L*. Apidologie, 24, 195–217.

Getz, W.M. and **Akers, R.P.** (1995) *Partitioning nonlinearities in the response of honey bee olfactory receptor neurons to binary odors*. BioSystems, 34, 27–40.

Getz, W.M. and **Akers, R.P.** (1997a) *Response of American cockroach (*Periplaneta americana*) olfactory receptors to selected alcohol odorants and their binary combinations*. J. Comp. Physiol. A, 180, 701–709.

Getz, W.M. and **Akers, R.P.** (1997b) *Coding properties of peak and average response rates in American cockroach olfactory cells*. BioSystems, 40, 55–63.

Getz, W.M. and **Lutz, A.** (1999) *A neural network model of general olfactory coding in the insect antennal lobe*. Chem. Senses, 24, 351–372.

Hilborn, R. and **Mangel, M.** (1997) The Ecological Detective: Confronting Models with Data. Princeton University Press, Princeton, NJ.

Hildebrand, J.G. and **Shepherd, G.M.** (1997) *Mechanisms of olfactory discrimination: converging evidence for common principles across phyla*. Annu. Rev. Neurosci., 20, 595–631.

Kaissling, K.-E. (1987) In Colbow, K. (ed.), R.H. Wright Lectures on Insect Olfaction. Simon Fraser University, Burnaby, British Columbia, Canada.

Kaissling, K.-E. (1998a) *Flux detectors versus concentration detectors: two types of chemoreceptors*. Chem. Senses, 23, 99–111.

Kaissling, K.-E. (1998b) *Pheromone deactivation catalyzed by receptor molecules: a quantitative kinetic model*. Chem. Senses, 23, 385–395.

Koester, J. (1991) *Membrane potential*. In Kandel, E.R., Schwartz, J.H., Jessell, T.M. (eds), Principles of Neural Science, 3rd edn. Elsevier, New York, pp. 81–103.

Lancet, D., Sadovsky, E. and **Seidemann, E.** (1993) *Probability model for molecular recognition in biological receptor repertoires: significance to the olfactory system*. Proc. Natl Acad. Sci. USA, 90, 3715–3719.

Lánsky, P. and **Rospars, J.** (1993) *Coding of odor intensity*. Biosystems, 31, 15–38.

Lánsky, P. and **Rospars, J.** (1999) *Odorant concentration and receptor potential in olfactory sensory neurons*. Chem. Senses, in press.

Lánsky, P., Rospars, J.-P. and **Vermeulen, A.** (19940 *Basic mechanisms of coding stimulus intensity in the olfactory sensory neuron*. Neural Process. Lett., 1, 9–12.

Lemon, W.C. and **Getz, W.M.** (1997) *Temporal resolution of general odor pulses by olfactory sensory neurons in American cockroaches*. J. Exp. Biol., 200, 1809–1819.

Malaka, R., Ragg, T. and **Hammer, M.** (1995) *Kinetic models of odor transduction implemented as artificial neural networks—simulations of complex response properties of honeybee olfactory neurons*. Biol. Cybernet., 73, 195–207.

Mascagni, M.V. and **Sherman, A.S.** (1998) *Numerical methods for neuronal modeling*. In Koch, C. and Segev, I. (eds), Methods in Neuronal Modeling: From Ions to Networks, 2nd edn. MIT Press, Cambridge, MA, pp. 569–606.

Masson, C. and **Mustaparta, H.** (1990) *Chemical information processing in the olfactory system of insects*. Physiol. Rev., 70, 199–245.

Moore, P.A. and **Atema, J.** (1991) *Spatial information in the three-dimensional fine structure of an aquatic odor plume*. Biol. Bull., 181, 408–418.

Murlis, J., Elkington, J.S. and **Cardé, R.T.** (1992) *Odor plumes and how insects use them*. Annu. Rev. Entomol., 37, 505–32.

Reed, R.R. (1994) *The molecular basis of sensitivity and specificity in olfaction*. Cell Biol., 5, 33–38.

Restrepo, D., Teeter, J.H. and **Schild, D.** (1996) *Second messenger signaling in olfactory transduction*. J. Neurobiol., 30, 37–48.

Rospars, J.P. (1988) *Structure and development of the insect antenno-deutocerebral System*. Int. J. Insect Morphol. Embryol., 17, 243–294.

Rospars, J., Lánsky, P., Tuckwell, H.C. and **Vermeulen, A.** (1996) *Coding of odor intensity in a steady-state deterministic model of an olfactory receptor neuron*. J. Computat. Neurosci., 3, 51–72.

Singer, M.S. and **Shepherd, G.M.** (1994) *Molecular modeling of ligand–receptor interactions in the OR5 olfactory receptor*. Neuroreport, 5, 1297–1300.

Smith, B.H. and **Getz, W.M.** (1994) *Nonpheromonal olfactory processing in insects*. Annu. Rev. Entomol., 39, 351–375.

Smith, B.H. and **Menzel, R.** (1989) *An analysis of variability in the feeding motor program of the honey bee; the role of learning in releasing a modal action pattern*. Ethology, 82, 69–81.

Smith, H. and **Waltman, P.** (1995) The Theory of the Chemostat. Cambridge University Press, Cambridge.

Trotier, D. (1994) *Intensity coding in olfactory receptor cells*. Cell Biol., 5, 47–54.

Tuckwell, H.C., Rospars, J., Vermeulen, A. and **Lánsky, P.** (1996) *Time-dependent solutions for a cable model of an olfactory receptor neuron*. J. Theor. Biol., 181, 25–31.

Vermeulen, A. and **Rospars, J.** (1998) *Dendritic integration in olfactory sensory neurons: a steady-state analysis of how the neuron structure and neuron environment influence the coding of odour intensity*. J. Computat. Neurosci., 5, 243–266.

Vermeulen, A., Rospars, J., Lánsky, P. and **Tuckwell, H.C.** (1996) *Coding of stimulus intensity in an olfactory receptor neuron: role of neuron spatial extent and passive dendritic backpropagation of action potentials*. Bull. Math. Biol., 58, 493–512.

Vickers, N.J. and **Baker, T.C.** (1994) *Reiterative responses to single strands of odor promote sustained upwind flight and odor source location by moths*. Proc. Natl Acad. Sci. USA, 91, 5756–5760.

Accepted May 25, 1999

Appendix

Glossary of symbols

Independent variable

t—time (scaled so that $k_2^* = 1$)

System variables

The dynamics of each variable is modeled by its own differential equation.

A—density of activated ligand–receptor complexes

B—density of 'bound-but-not-yet-activated' ligand–receptor complexes

L—density of free ligands available for binding

M—density of 'enabling molecules' facilitating the ligand–receptor activation process

V—membrane voltage of olfactory receptor neuron

Auxiliary variables

R—density of membrane receptors normalized to 1 so that all related densities are in 'membrane-receptor-density' units

$L_{\text{in}}(t)$—ligand input flux as a function of time t

$S(t)$—spike rate of olfactory receptor neuron as a function of time t

$\overline{S}(t_1,t_2)$—average spike rate over the interval $[t_1,t_2]$

U—density of unbound receptors, $U = R - B - A$

Rate parameters

a_0—rate at which membrane voltage decays back to resting state
a_1—rate at which membrane voltage depolarizes
a_2—rate at which membrane voltage hyperpolarizes (two pathway model only)
k_0—rate at which ligands enter the perireceptor space; if it is assumed that $k_0 \to \infty$, this is equivalent to assuming $L(t) = L_{in}(t)$
k_{-0}—rate at which ligands exit the perireceptor space; it is assumed $k_{-0} = 0$—positive k_{-0} is not needed to prevent the pooling of active ligands in the perireceptor space because, after dissociating from receptors, ligands are assumed to be transformed to a degraded state
k_1—rate at which ligand and receptors associate to form a bound-but-not-yet-activated complex
k_{-1}—rate at which bound-but-not-yet-activated ligand–receptor complexes disassociate
k_2*—maximum rate at which bound-but-not-yet-activated ligand–receptor complexes become activated; the actual activation rate k_2 is a function of the enabling molecule density M [see equation (4) below]; note that time is scaled so that k_2* = 1
k_{-2}—rate at which activated ligand–receptor complexes disassociate to leave behind a degraded ligand molecule
k_3—rate at which enabling molecules are replenished when their density is very low
k_{-3}—rate at which enabling molecules are used in ligand–receptor activation process

Scaling parameters

M_0—resting or saturation density for enabling molecules
$M_{1/2}$—half-saturation or Michaelis–Menten constant in the Monod activation rate function $k_2(M/B)$ (see equation 4)
S_{max}—maximum spiking rate (set to 200 spikes/s)
t—spike generation time delay
V_{rest}—cell membrane resting voltage (set to –50 mV)
V_{dep}—maximum voltage to which cell membrane can be depolarized (set to +50 mV)
V_{crit}—depolarization threshold for spiking to occur
V_{hyp}—minimum voltage to which cell membrane can be hyperpolarized

Model equations

From the processes described in the text, it follows that the kinetic equations for L, B and A are (Lánsky and Rospars, 1999)

$$\frac{dL}{dt} = k_0(L_{in} - L) - k_1 L(R - B - A) \tag{1}$$

$$\frac{dB}{dt} = k_1 L(R - B - A) - (k_{-1} + k_2)B + k_{-2}A \tag{2}$$

$$\frac{dA}{dt} = k_2 B - k_{-2}A \tag{3}$$

For the case where the association rate k_2 is a Monod function of the ratio M/B rather the density M itself we have:

$$k_2 = \frac{k_2^* M(t)}{M_{1/2}B(t) + M(t)} \tag{4}$$

[The time argument t on the right-hand side is included to stress that k_2 varies with time as M and B vary with time. Note that ratio M/B does not appear explicitly on the right-hand side of equation (4) because we have multiplied the top and bottom by B.]
From the assumptions in the text, the density M of these enabling molecules is modeled by the equation

$$\frac{dM}{dt} = k_3\left(1 - \frac{M}{M_0}\right) - k_{-3}k_2 B \tag{5}$$

The dynamics of the membrane voltage depends on the current voltage state and the number of activated receptors and is modeled by the equation

$$\frac{dV}{dt} = \alpha_0(V_{rest} - V) + \alpha_1 A(t)(V_{dep} - V) \tag{6}$$

A clipped linear time-delay relationship between voltage and spiking rate, as described in the text, is given by

$$S(t) = \frac{(V(t-\tau) - V_{crit})}{(V_{dep} - V_{crit})} S_{max} \text{ for } V > V_{crit} \text{ and 0 otherwise} \tag{7}$$

Hence the average spiking rates over intervals $[t_1, t_2]$ is

$$\overline{S}(t_1, t_2) - \frac{S_{max}}{(t_2 - t_1)(V_{dep} - V_{crit})} \int_{t_1}^{t_2} \max\{0, V(t-\tau) - V_{crit}\} dt \tag{8}$$

In the case where two pathways exist, each satisfying a set of equations (1)–(5) that determine the densities of corresponding activated ligand–receptor complexes $A_1(L_1,t)$ (depolarizing pathway) and $A_2(L_2,t)$ (hyperpolarizing pathway), then the membrane voltage will be governed by the equation

$$\frac{dV}{dt} = \alpha_0(V_{rest} - V) + \alpha_1 A_1(L_1,t)(V_{dep} - V) + \alpha_2 A_2(L_2,t)(V_{hyp} - V) \tag{9}$$